Theor Chem Acc (2007) 117:1061–1072
DOI 10.1007/s00214-006-0220-3

REGULAR ARTICLE

Complex excited dynamics around a plateau on a retinal-like potential surface: chaos, multi-exponential decays and quantum/classical differences

Fabrizio Santoro · Alessandro Lami · Massimo Olivucci

Received: 24 July 2006 / Accepted: 13 October 2006 / Published online: 10 January 2007

Abstract We investigate the classical and quantum dynamics on the plateau of an excited potential energy surface (PES) whose shape mimics the PES driving the photoisomerization of the protonated Schiff base of retinal (PSBR). We adopt a two-dimensional analytical model of the PES, and perform an extended study by varying the potential parameters, revealing a scenario whose interest goes beyond the relevance for the specific case of PSBR. In fact, we document cases with net differences among classical and quantum dynamical predictions, for barrierless PESs. Classical trajectories released on the PES display the signature of chaos and partial trapping on the plateau, whose origin is purely dynamical, since no barrier exists. At variance, on the same barrierless PESs, quantum dynamics does not predict any trapping, always showing a complete depletion of the excited population according to an approximate mono-exponential law. The plateau on the PES promotes complex and unusual dynamical features, and it is sufficient to introduce a very small barrier along the *cis–trans* torsional mode to give rise to a multi-exponential decay, also at quantum level. Our results are of general interest because plateaux are often found in the excited states of conjugated chromophores.

Keywords Wavepacket dynamics · Chaos · Dynamical trapping · Multi-exponential decay

Electronic supplementary material The online version of this article (doi:10.1007/s00214-006-0220-3) contains supplementary material, which is available to authorized users.

F. Santoro · A. Lami
Istituto per i Processi Chimico-Fisici,
Area della Ricerca del CNR di Pisa,
Via Moruzzi 1, 56124 Pisa, Italy
e-mail: f.santoro@ipcf.cnr.it

A. Lami
e-mail: lami@ipcf.cnr.it

M. Olivucci
Dipartimento di Chimica dell'Università di Siena,
via A. Moro 2, 53100 Siena, Italy

M. Olivucci (✉)
Chemistry Department, Bowling Green State University,
Bowling Green, OH 43403, USA
e-mail: molivuc@bgnet.bgsu.edu

M. Olivucci
Centro per lo Studio dei Sistemi Complessi,
Via Tommaso Pendola 37, 53100 Siena, Italy
e-mail: olivucci@unisi.it

1 Introduction

The progress in the field of theory of electronic structure together with the continuous increase in computational resources makes possible to describe with accuracy the excited potential energy surfaces (PES) of medium-size molecules undergoing true chemical photoreactions. State of the art studies are therefore bringing to light the complexity and richness of real-molecule excited PESs, showing a wealth of unusual features as wide plateaux [1–4], very low barriers, long and curved intersection seams among PESs [5,6], and even truly multidimensional intersections seams [7]. Such complex features might have very important dynamical consequences leading to new effects with respect to those commonly met in ground-state reactivity. As an example, crossing long intersection seams at different points could have a deep impact in photoisomerizations, while very low

energy barriers could allow sensible tunnelling effects also for atoms heavier than hydrogen.

To improve our general understanding on these phenomena, it is important to individuate and bring to light general and transferable effects, encompassing the gap between the level of "working knowledge" obtained till now for ground-state and excited-state reactions. Hopefully, such a working knowledge will in the near future, help the chemical design and engineering of molecules for the control of their excited-state reactions, with possible enormous applications in several areas of nanotechnology, from molecular motors and devices to molecular wires and artificial light antenna.

Wide plateaux seem to be a common feature in excited PES of molecules with extended π-systems [1–4]. They have been described with highly accurate CASSCF method for several models of protonated Schiff base of the retinal chromofore (PSBR) [1–3], but have also been predicted for the excited PES of thiacyanine [4], and probably exist also in the π/π^* PES of DNA bases as uracils (R. Improta and F. Santoro, unpublished results). We have shown that a very small barrier (200 cm^{-1}) on the plateau of PSBR can switch the excited population depletion from mono- to bi-exponential [8], providing a plausible explanation for the experimental evidences [9–13].

CASSCF calculations [1–3] have shown that the excited state (S_1) branch of the reaction coordinate in PSBR is dominated by a sequential progression along two nuclear modes that ultimately leads to a conical intersection (CI) between the excited (S_1) and the ground (S_0) PES. More specifically, the structural evolution of PSBR along the torsion describing the *cis* to *trans* change is preceded by relaxation of the initial Franck–Condon (FC) structure along a collective C–C stretching mode of the chromophore backbone toward an energy plateau (SP). This result is in line with several experimental results for the chromofore in solution and in protein environment [14–19]. Cembran et al. [20] have shown that the essential features of the S_1 PES of PSBR are reproduced by the simple analytical potential V^C (plotted in Fig. 1):

$$V^C(x_s, y_t) = 1/2 m_s \omega_s^2 x_s^2 - 1/2 m_t \omega_t^2 x_s y_t^2, \quad (1)$$

where x_s and y_t are the stretching and torsion coordinates, respectively; m_s and m_t, their masses; and ω_s and ω_t, their frequencies.

The initial wave packet is located at $y_t = 0$ and at a negative x_s value, fixed so to reproduce the 6 kcal mol^{-1} energy gap between the FC and SP point predicted via ab initio computations [2]. Due to the dependence on x_s, V^C is bound along y_t (i.e. acceleration toward $y_t = 0$) when $x_s < 0$, while it is unbound (i.e. acceleration toward large y_t values) when $x_s > 0$. This highly anharmonic feature creates the plateau around the origin (SP) whose existence has been documented, via ab initio MEP mapping for realistic PSBR models [3].

In the present paper, we investigate in detail the dynamics on the plateau described by the model in Eq. (1) by an extended study covering a wide range of the PES parameters, comparing classical and quantum dynamics results. Our results show that the plateau is the origin of a very complex classical dynamical behaviour, which can cause partial trapping even if the PES is barrierless and chaotic, and we document a strict correlation between these two phenomena: regular trajectories are those giving rise to trapping, while chaotic trajectories are not trapped. For some choice of the PES parameters, the complexity of the dynamics reflects in a marked difference between the classical and quantum predictions. Finally, the results here presented attribute a general validity to the observation made in [8] for the particular case of PSBR (ω_s = 1,500 cm^{-1} and ω_t = 200 cm^{-1}), suggesting that the occurrence of a small barrier on a plateau of an excited PES (due to intra-molecular or environmental factors) can easily switch the quantum population decay law from mono- to multi-exponential.

2 Computational methods

We study the dynamics on the plateau of the V^C potential. When suitable values for the parameters are chosen, V^C reproduces the essential features of the excited PES of PSBR, i.e., the FC and SP region and the existence of two decaying channels which open along y_t for $x_s > 0$. It does not describe the region of the CI, which must be thought of to be somewhere in the decaying channels. Below we assume that, once entering into these channels, the wave packet irreversibly proceeds toward the CI. Very interesting experimental information on the molecular structure at the conical intersection of PSBR has been reported by the group of Mathies [21].

Classical trajectories are obtained integrating the classical Hamilton's equation of motion using a code written within the Mathematica package environment. Quantum calculations are performed using a home-made program and assuming the simple kinetic operator $T = (2m_s)^{-1}\partial^2/\partial x_s^2 + (2m_t)^{-1}\partial^2/\partial y_t^2$. We use the Fourier method [22], representing the wave packet on a bi-dimensional 324 × 324 grid of points defined in the range $-3.5\,au \leqslant x_s \leqslant 14\,au$ and $-14\,au \leqslant y_t \leqslant 14\,au$ ($m_s = m_t = 1\,amu$), and computing the kinetic integrals by fast Fourier transform FFT. The propagation

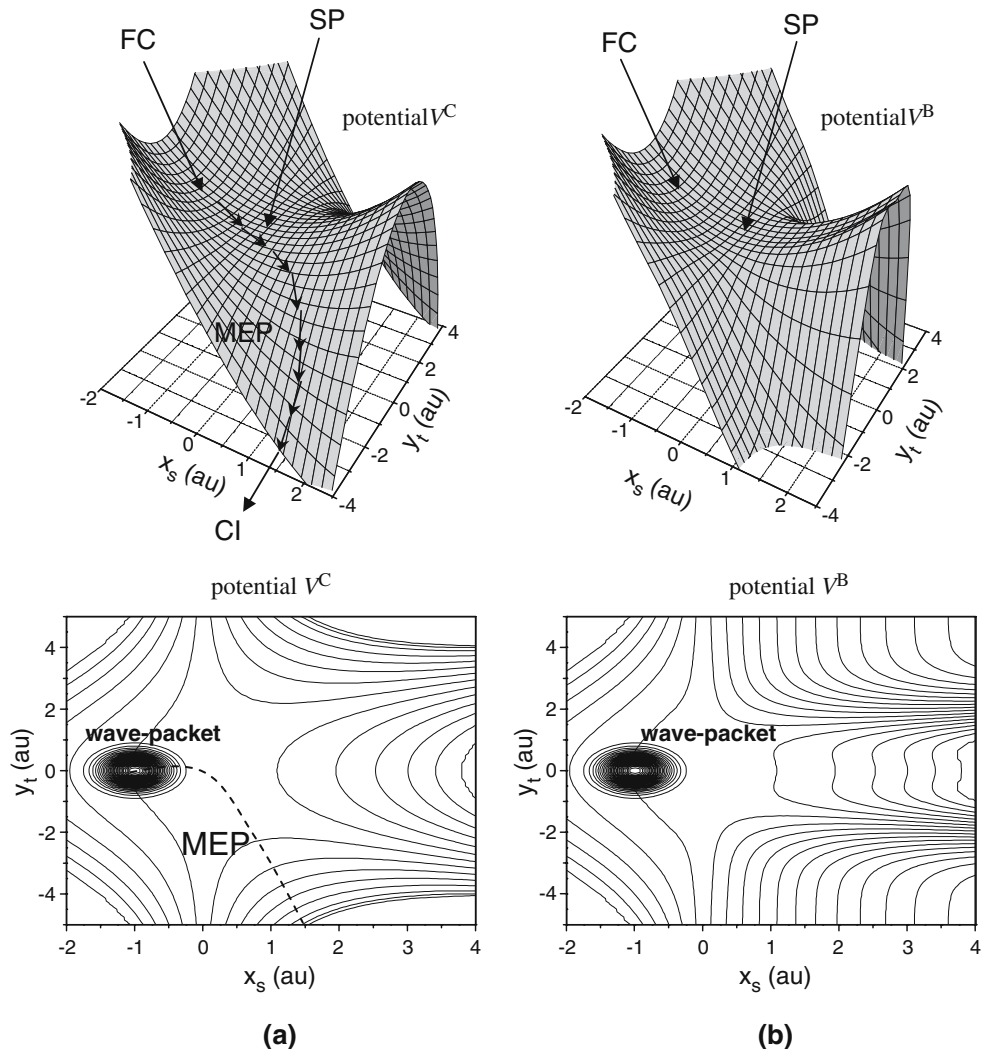

Fig. 1 3D plot and contour plot of **a** potential V^C and **b** potential V^B. In the contour plot, superimposed to the potential we also report the $|FC\rangle$ wave packet at $t = 0$. In **a** the *arrows* and the *dashed line* sketch the MEP toward negative values of y_t, but notice that due to the potential symmetry an equivalent MEP develops toward positive values of y_t

is accomplished by an orthogonalized-Lanczos method [23,24].

The increasing acceleration toward larger y_t in the region $x_s > 0$, prompted by the shape of the PES in Eq. (1), rises technical problems in both the classical and quantum calculations. In the former case, the necessary propagation step in the numerical solution of equation of motion becomes exceedingly small, while in the latter case, a very dense grid would be needed to reproduce the acquired kinetic energy. Actually the potential V^C in Eq. (1) is interesting for our scopes only in the plateau region, i.e. in a limited range of torsional angles around the equilibrium value $y_t = 0$, and the acceleration at large y_t (for $x_s > 0$) is only important as much as it causes an irreversible motion toward the CI, once the decay channel has been entered. Thus, for classical trajectories, the numerical problem was solved stopping each trajectory as soon as it reaches a $|y_t|$ value, from which it can be safely assumed that it will not go back to the plateau region. For quantum calculations, the problem is solved by transforming the potential in the uninteresting region, so that it becomes flat. This is accomplished by defining a new potential $V_Q^C(x_s, y_t)$ by means of a switching function $(E_1 + V^C(x_s, y_t) \exp[\alpha_Q R])/(1 + \exp[\alpha_Q R])$, with $R = V^C(x_s, y_t) - E_2$. $V_Q^C(x_s, y_t)$ is identical to $V^C(x_s, y_t)$ when $V^C(x_s, y_t) \gg E_2$ and assumes the constant value E_1 when $V^C(x_s, y_t) \ll E_2$. The chosen parameters $E_2 = -35{,}000$ cm^{-1}, $E_1 = -45{,}000$ cm^{-1} and $\alpha_Q = 0.001$ cm assure that $V_Q^C(x_s, y_t)$ differs from $V^C(x_s, y_t)$ only in a region where the wave packet is so accelerated that it never comes back to the SP region.

Because of that, on the following, we will generally refer to both of them as V^C. In the flat region the wave packet is progressively and very slowly absorbed to avoid unphysical effects at the borders of the grid. This is accomplished by multiplying the wavefunction by the function $A_{xs}(x_s)A_{yt}(y_t)$ [25] with

$$A_p(p) = \begin{cases} 1 & p^{\min} < p > p^{\max}, \\ \exp(-C_{abs}^{p\,\min}(p-p^{\min})^2) & p < p^{\min}, \\ \exp(-C_{abs}^{p\,\max}(p-p^{\max})^2) & p > p^{\max}, \end{cases} \tag{2}$$

where $p = x_s, y_t$, $x_s^{\min} = \infty$, $x_s^{\max} = 5.9$ au, $C_{abs}^{s\,\max} = 0.0011$ au, $y_t^{\min} = -5.9$ au, $y_t^{\max} = 5.9$ au, $C_{abs}^{t\,\min} = C_{abs}^{t\,\max} = 0.0011$ au. We have tested the convergence of the quantum results with respect to the size and the number of points of the grid and to the rate of absorption of the wave packet.

3 Results

3.1 Motion of classical trajectories with variable initial position along y_t

In Cembran et al. [20] it is shown that classical trajectories released on V^C ($\omega_s = 711$ cm^{-1} and $\omega_t = 503$ cm^{-1}) at $x_s = -1$ au (corresponding to an FC–SP energy gap of 6 kcal/mol) and at different values of y_t with zero initial momenta fall into two different categories: the ones that remain permanently (or for a very long time) trapped in the SP region and are non-reactive (i.e. do not lead to a permanent *cis–trans* displacement) and the ones that quickly escape toward large y_t values and (are assumed to) reach the CI, where they decay to the S_0 energy surface. Here, we choose the lines $y_t \pm 4$ au as borders between the non-reactive (NR) region ($|y_t| \leqslant 4$ au, including the FC and SP points) and the reactive (R) region ($|y_t| > 4$ au, the decay channels irreversibly driving to CI) and compute the time τ spent by a single trajectory in NR before crossing the borders, as a function of the initial position $y_t(0)$. The results obtained propagating the trajectories up to 20 ps, are reported in Fig. 2 and show a striking dependence of τ on the initial position (we have exploited the fact that the PES is an even function of y_t and scanned only the region of positive $y_t(0)$ for the range of initial positions $0 < y_t(0) < 1$ au with steps of 0.01 au).

First, notice that the trajectory with $y_t(0) = 0$ is unique, since it never acquires momentum along y_t and is obviously non-reactive. However, in the nearby region around $y_t(0) = 0$, τ varies drastically with $y_t(0)$, being for example 430 fs at $y_t(0) = 0.07$ au and at $y_t(0) = 0.2$ au,

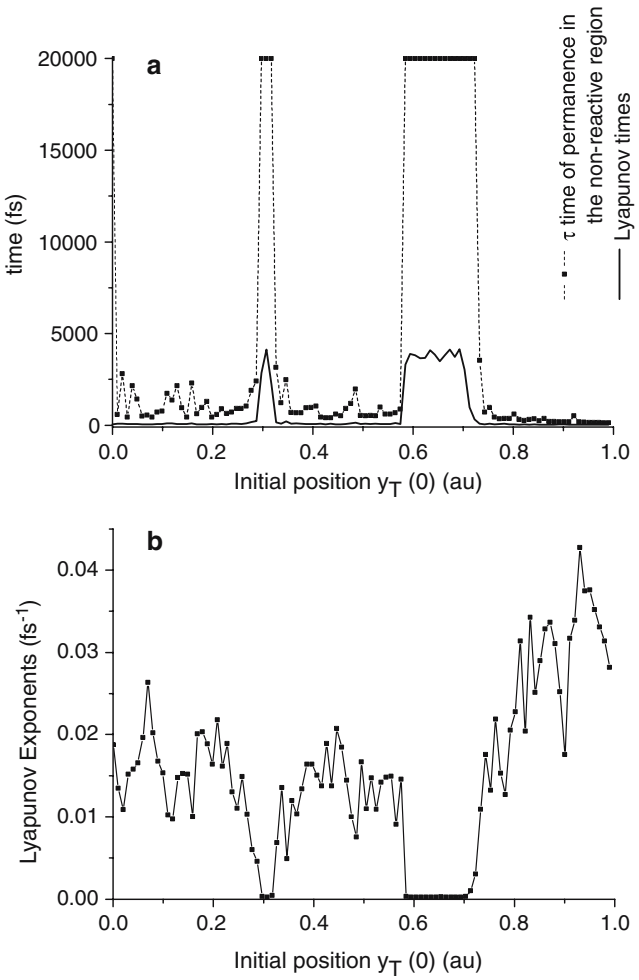

Fig. 2 Results of the dynamics of a set of trajectories with zero initial momenta $x_s(0) = -1$ au and $y_t(0)$ variable from 0 to 1 au (i.e. the region spanned by $|FC\rangle$ at $t = 0$, see Fig. 1) with steps of 0.01 au: **a** time of permanence in the non-reactive region (*squares, dot line*) and Lyapunov times (the inverse of Lyapunov exponents, *full line*); **b** Lyapunov times. Computed values are indicated by the *squares* while the interpolating lines are only reported for better visualization

while it is 2,850 fs at $y_t(0) = 0.1$ au. When the analysis is extended toward larger $y_t(0)$ values, even more remarkable results come out. In fact, while in the region around $y_t(0) = 0.3$ au and $y_t(0) = 0.58 - 0.75$ au τ exceeds the maximum propagation time 20 ps (and this explains the flat part of the graph in Fig. 2a), it is only 570 fs at $y_t(0) = 0.55$ au and it is always lower than 350 fs for $y_t(0) > 0.8$ au.

These features strongly suggest that, due to the topology of V^C, the decay of a wave packet starting at FC can be characterized by different time regimes. While the reason for the question why a fraction of the trajectories escape accelerating along y_t is intuitive, the trapping mechanism is subtle. In mechanistic terms such

behaviour originates from the fact that in the $x_s > 0$ region, a classical particle feels a force toward large y_t but also toward $x_s = 0$. Thus, trajectories that do not escape in time from the NR region (i.e. do not accelerate enough along y_t while crossing the half-plane $x_s > 0$) go back to the bound region $x_s < 0$, where they feel a compression force toward $y_t = 0$. For given initial conditions, such a mechanism repeats at each oscillation along x_s resulting in a dynamical trapping.

3.2 Instability and dynamical chaos

The trajectories described above are extremely sensitive to the initial conditions and to the values of the parameters of the PES. For instance, while τ is 2,850 fs for $y_t(0) = 0.1$ au, it is only 1,180 fs if one shifts the initial condition by 1% $y_t(0) = 0.101$ au. Also, a slight change of the potential V^C could have a dramatic effect. In fact changing ω'_s by 1% (i.e. from 711 to 718 cm^{-1}) for $y_t(0) = 0.1$ au, causes a change in τ of 60% (2,850 to >1,130 fs). The effect is still larger if we instead perturb ω'_t by 1% (from 503 to 508 cm^{-1}) getting $\tau = 430$ fs: a decrease of a factor 6.6.

These features suggest that the dynamics is chaotic and that there is a correlation between high τ values and better stability with respect to perturbations. To test this hypothesis, we computed the Lyapunov exponents for the same set of 101 trajectories for which we calculated τ in Fig. 2a, following the method of Benettin et al. [26] and stopping the procedure when the single trajectory was still in the NR region. The obtained values are approximate (but fully adequate for our scopes) since it was not always possible to reach a full convergence of the $t \to \infty$ limit that defines the Lyapunov exponents, most of all for the trajectories that quickly escape the non-reactive region. The Lyapunov exponents are reported in Fig. 2b, while their inverses, the Lyapunov times (i.e. the time constant for the exponential divergence) are reported in Fig. 2a (solid line), together with τ. Lyapunov exponents are always >0 (chaos), but their magnitude varies greatly and is clearly correlated with τ, being larger (faster exponential divergence of close trajectories) in the region where τ is shorter. Therefore, regular (chaotic) trajectories are those which remain (do not remain) trapped in the NR region. Notice that also the trajectory at $y_t(0) = 0$ au, which has trivially an infinite τ, is chaotic and a very slight change in $y_t(0)$ leads to a quick escape from the NR region. Further insight in to the problem could come from an application of the quasiperiodic orbit analysis proposed by Stock et al. [27,28].

3.3 Classical simulation of the wave packet motion

We turn now to study the dynamics of the 2D wave packet $|FC\rangle$ assuming that the system, initially in the ground (harmonic) vibrational state of the S_0 surface, is vertically excited to S_1 by a sufficiently short laser pulse. A bunch of classical trajectories representative of $|FC\rangle$ is obtained choosing the initial conditions according to the Wigner distribution (WD) and checking the convergence of the desired observables with respect to the number of the trajectories. For the present case, the WD is simply the product of the square modulus of the vibrational wave function in the coordinate and in the momentum space for each coordinate,

$$\begin{aligned} W(x_s, p_{xs}, y_t, p_{yt}) &= N_s N_t \exp[-(x_s - x_s(0))/2\sigma_s^2 - 2\sigma_s^2 p_s^2] \\ &\quad \times \exp[-(y_t - y_t(0))/2\sigma_t^2 - 2\sigma_t^2 p_t^2], \end{aligned} \tag{3}$$

where N_s and N_t are normalization constants, $\sigma_s = 1/\sqrt{2m_s\omega_s}$, $\sigma_t = 1/\sqrt{2m_t\omega_t}$ and $(x_s(0), y_t(0)) = (-1\,\text{au}, 0\,\text{au})$ is the FC point.

For each simulation we ran 1,000 trajectories for a time interval of 1 ps, and checked the convergence of the results by increasing the number of trajectories. Since we are interested in how the $|FC\rangle$ moves into the SP $\to$CI channel, we monitor the S_1 wave packet population decay out of the NR region. This is computed as $P_{NR}(t) = 1 - F_{TI}(t)$ where $F_{TI}(t)$ is the time-integrated flux $F_{TI}(t)$ along the borders $y_t \pm 4$ au. Different time regimes in the motion toward the CI would reflect into a multi-exponential decay of the $P_{NR}(t)$ population.

$F_{TI}(t)$ at time t is classically computed as the fraction of trajectories that have crossed the lines at $y_t \pm 4$ au in the time interval $[0, t]$. This recipe is completely equivalent to adopting a semi-classical initial-value representation (IVR) of the propagator, and then to performing the evaluation of the observable in the linearized approximation (LSC-IVR) [29]. As it is well known, this approximation can reproduce many quantum features but it fails when tunnelling is important [30]. This comment will be of relevance in the following discussion.

For the sake of simplicity, we consider cases in which there is no frequency shift for the two modes after the transition from $S_0(\omega'_s, \omega'_t)$ to $S_1(\omega_s, \omega_t)$. Thus, we use $\omega_t = \omega'_t = 503$ cm^{-1} and $\omega_s = \omega'_s = 711$ cm^{-1}.

Figure 3 (line 1) reports the result for $P_{NR}(t)$ obtained with trajectories whose initial conditions sample the correct coordinates and momenta WD, and compares it with the result (line 3) obtained sampling only the wave packet coordinate distribution (CD) and imposing null initial momenta to both coordinates (i.e. $p_s(0) = 0$ and $p_t(0) = 0$), a 2D extension of the situation considered in

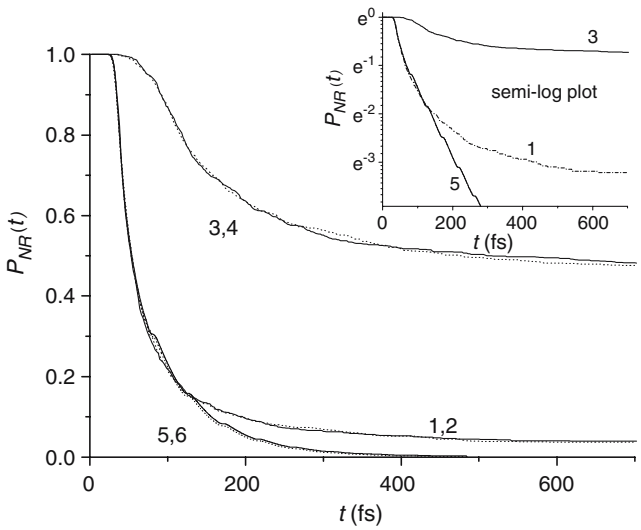

Fig. 3 Population decay of the non-reactive wave packet. *Lines 1 and 3,* refer to classical-trajectories simulations with initial momenta distributed according to the Wigner distribution *(1)* or equal to zero *(3)*. *Line 5* reports quantum results. *Lines 2, 4, 6* are obtained as *1, 3, 5* only changing ω_t from 503 to 508 cm^{-1}. In the inset, semi-log plot of the *lines 1, 3 and 5*

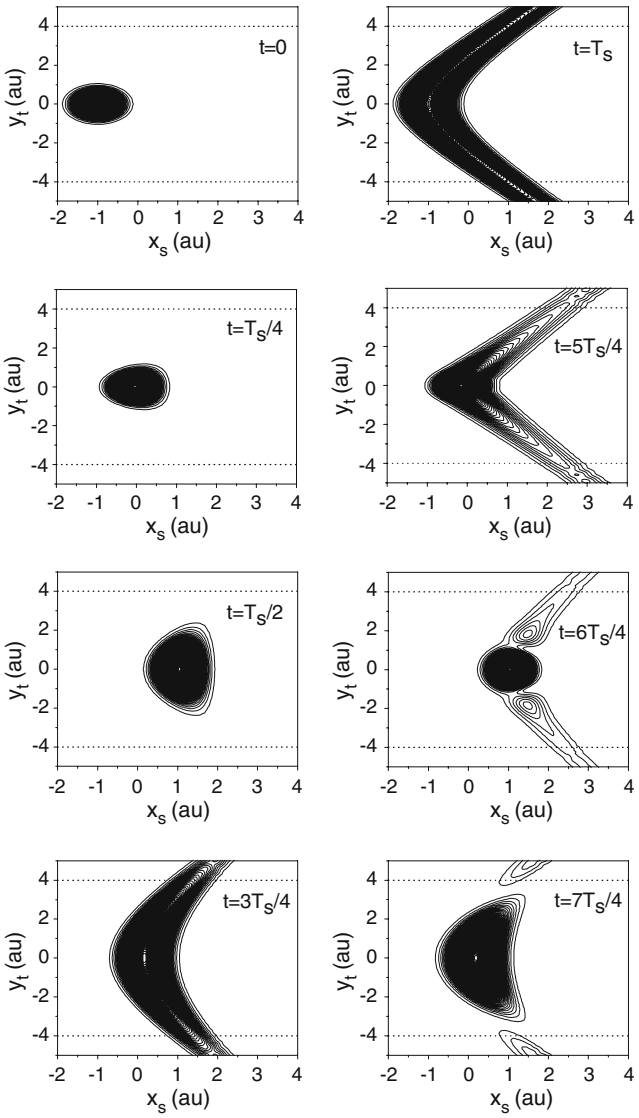

Fig. 4 Snapshots of the quantum wave packet running on V^C at different times, reported as fractions of the stretching period T_s. Notice that for a better comparison, before plotting, the part of the wave packet not yet absorbed at the borders of the grid has been re-normalized (see Supporting Material for the normalization factors)

Sects. 3.1 and 3.2 and in ref. [20]. Line 3 shows clearly a non mono-exponential decay of $P_{NR}(t)$ for the CD case, which is stressed also by the semi-log plot in the inset of Fig. 3: after an induction time, about one half of the trajectories (and hence of the wave packet) crosses the borders quickly, while the other half remains trapped in the NR region and/or escapes from it much more slowly. At this point, we stress that a permanent trapping could turn into a slow decay when taking into account the perturbation due to the interaction with other intramolecular modes or with the solvent.

Line 3 shows that even considering the proper 2D coordinate-distribution of $|FC\rangle$ (CD), two clearly different time regimes can be distinguished in its dynamics, as suggested by the 1D analysis in [20]. This behaviour changes drastically when we take into account the correct WD momenta distribution (line 1) of $|FC\rangle$. In fact, in this case, the major part of the wave packet decays according to a single exponential, while only a residual part decays more slowly or is trapped in the plateau region. This also shows that the effectiveness of the dynamical trapping is strongly decreased by introducing a momentum distribution in the bunch of trajectories, which is a further step in mimicking the quantum behaviour.

Lines 2 and 4 are analogous to lines 1 and 3, respectively, from which they differ because here $\omega_t = 508$ cm^{-1}. In Sect. 3.2 we showed that such a slight change (1%) has a dramatic effect on the dynamics of the trajectories with null initial momenta and $x_s(0) = -1$ au. Figure 3 shows that the high sensibility evidenced by single trajectories to the parameters of the PES is strongly reduced when one considers a representative ensemble of trajectories.

3.4 Quantum wave packet dynamics

Lines 5 and 6 of Fig. 3 report the results of the exact quantum dynamics of $|FC\rangle$ for the parameters $\omega_t = \omega'_t = 503$ cm^{-1} and $\omega_t = \omega'_t = 508$ cm^{-1}. Comparison of lines 3 and 5 shows that the WD classical bunch

Table 1 Exponential fits of quantum $P_{NR}(t)$ for different choices of the S_1 potential

Potential	k^a	B^{max}	τ_0^b	Mono-exponential Fit[c]	Bi-exponential Fit[d]
V^C	1	0	28	$\tau_1 = 47$	$A_1 = 0.50 \quad \tau_1 = 22$
					$A_2 = 0.50 \quad \tau_2 = 80$
				$\chi^2 = 7.2 \times 10^{-4}$	$\chi^2 = 1 \times 10^{-4}$
V^C	1.2	0	26	$\tau_1 = 73$	$A_1 = 0.48 \quad \tau_1 = 32$
					$A_2 = 0.52 \quad \tau_2 = 124$
				$\chi^2 = 1.2 \times 10^{-3}$	$\chi^2 = 1.2 \times 10^{-4}$
V^C	1.6	0	27	$\tau_1 = 107$	$A_1 = 0.59 \quad \tau_1 = 56$
					$A_2 = 0.41 \quad \tau_2 = 214$
				$\chi^2 = 1.6 \times 10^{-3}$	$\chi^2 = 1.6 \times 10^{-4}$
V^B	1	205	21	$\tau_1 = 136$	$A_1 = 0.25 \quad \tau_1 = 16$
					$A_2 = 0.75 \quad \tau_2 = 184$
				$\chi^2 = 2.3 \times 10^{-3}$	$\chi^2 = 7.8 \times 10^{-5}$
V^B	1	475	21	$\tau_1 = 272$	$A_1 = 0.20 \quad \tau_1 = 17$
					$A_2 = 0.80 \quad \tau_2 = 362$
				$\chi^2 = 3.2 \times 10^{-3}$	$\chi^2 = 9.0 \times 10^{-5}$

Maximum barriers (B^{max}) in cm^{-1}, time constants in fs
[a] $\omega_s = k \times 711\ cm^{-1}, \omega_t = 503\ cm^{-1}$
[b] τ_0 induction time not considered in the fit (in femtoseconds)
[c] $f(t) = \exp(-(t-\tau_0)/\tau_1)$. Fitted from $t = \tau_0$
[d] $f(t) = A_1 \exp(-(t-\tau_0)/\tau_1) + A_2 \exp(-(t-\tau_0)/\tau_2)$. $A_1 + A_2 = 1$, fitted from $t = \tau_0$

of trajectories reproduces the dynamics of the quantum wave packet up to about 80 fs. Later, the exact quantum results show a faster decay and no dynamical trapping at all. Semi-log plot suggests a substantial mono-exponential decay. Table 1 actually documents that a bi-exponential fit allows some improvement with respect to the mono-exponential one, predicting two equal amounts of population decaying with time constants which differ by less than a factor 4. We conclude that the mere existence of the plateau on the potential V^C causes some marks of a bi-exponential decay also at quantum level, but they are modest (as confirmed by the plots of the fits reported in Supporting Materials, SM). Comparison of lines 5 and 6 indicates that in the quantum system the sensitivity to the exact parameters of the potential is lost.

Wave packet snapshots. Further insight into the wave packet quantum dynamics can be gained by the inspection of a set of snapshots. In Fig. 4, we report the contour lines of the probability density of $|FC\rangle$ in the coordinate space; the time step at which the snapshots are taken is a quarter of the oscillation period $T_s = 46.9$ fs of the stretching x_s, whose motion intuitively represents a kind of clock for the reaction, bringing periodically the system in the bound ($x_s < 0$) and unbound ($x_s > 0$) region. The total time-window covers two complete oscillations along x_s. At $t = 0$ $|FC\rangle$ is the expected 2D gaussian centred at $x_s = -1.0$ au and $y_t = 0$ au. At $t = T_s/4$ there is a crossing to the unbound region, while at $t = T_s/2$ $|FC\rangle$ reaches a turning point at about $x_s = 1.0$ au. In the mean time the wave packet starts elongating along the torsion but, in agreement with Fig. 3, at $t = T_s/2$ no significant part of it has yet crossed the borders of the NR region ($P_{NR}(T_s/2) = 1.00$). At later times, the central part of $|FC\rangle$ goes backward along x_s and $t \approx 3T_s/4$ it is re-entering the bound region where it reaches the left turning point at $t = T_s$. It is very interesting to note that in this second-half period (i.e. while the central part of $|FC\rangle$ is going back to the bound region) its wings keep on their run in the unbound region, toward the borders of the NR region; as a consequence, the wave packet drastically elongates and $P_{NR}(t)$ starts decaying (it is 0.88 at $t = 3T_s/4$ and 0.6 at $t = T_s$). At the beginning of the second period $|FC\rangle$ moves once more toward the unbound region while the wings keep elongating up to $t = 6T_s/4$. Indeed, at this time they are almost completely divided from the central part of the wave packet that still appears nicely localized. In the following quarter of period, the surviving part of $|FC\rangle$, still in the unbound region, starts elongating once more along y_t and in the last quarter of the second period its wings keep on their motion toward the decay channels while the central part goes back to the left turning point. At $t = 2T_s$ $P_{NR}(t) = 0.34$ and thus 66% of the initial wave packet has already moved out of the NR region. Even if the pictures would suggest a variable decay-rate of $P_{NR}(t)$ within each period, this comes out to be a distortion due to the impossibility to plot a continuous movie of the $|FC\rangle$ motion instead of a set of snapshots. In fact as shown in Fig. 3, after a first induction time, the $P_{NR}(t)$ decay appears pretty much as a mono-exponential func-

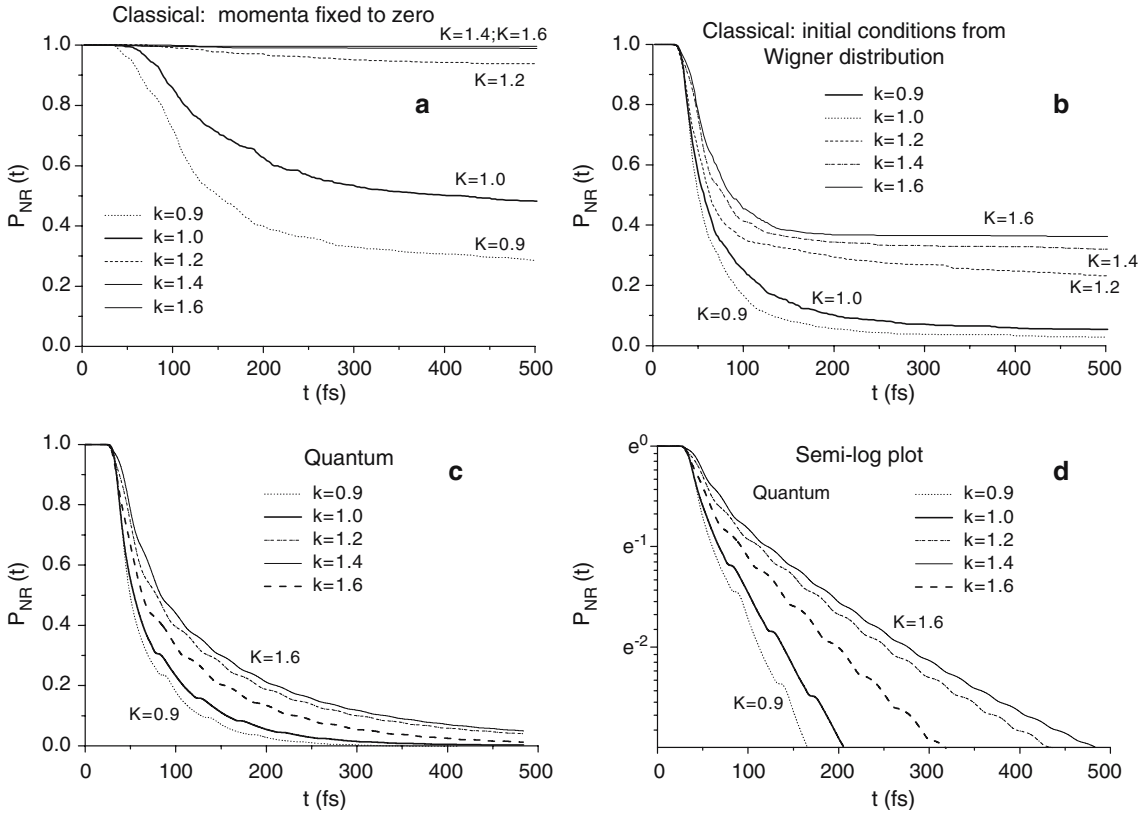

Fig. 5 Effect on the decay of the non-reactive wave packet population, obtained multiplying the stretching frequency, $\omega_s = 711\ cm^{-1}$, by Factor k; **a** and **b** classical-trajectories simulations with initial momenta equal to zero *(CD)* **a**, or distributed according to the Wigner distribution *(WD)* **b**; **c** quantum results; **d** semi-log plot of the quantum results. Notice in panel **d** that some marks of a bi-exponential decay exist but are moderate

tion of time, with only very small plateaux separated in time by $\sim T_s$. The snapshots taken during the third oscillation period along x_s are very much similar to those of the second period. The close similarity of the wave packet motion at each period is nicely consistent with a mono-exponential decay of $P_{NR}(t)$.

3.5 Effect of a change in the parameters of the potential

According to quantum dynamics, the $P_{NR}(t)$ decay is approximately mono-exponential and no trapping occurs for the V^C parameters selected in [20]. In view of the model study pursued here we investigated if by changing the PES parameters, but always considering barrierless surfaces, a quantum trapping could be observed. Thus, we altered the ratio between the frequencies of the two nuclear modes, by keeping fixed ω_t and ω'_t at 503 cm^{-1} and defining $\omega_s = \omega'_s = k \times 711\ cm^{-1}$ with $k = 0.9, 1.0, 1.2, 1.4, 1.6$. The results for $P_{NR}(t)$ are reported in Fig. 5 for the cases where the computation is performed for a bunch of classical trajectories with null momenta CD (a panel), according to WD (b panel) or using wave packet quantum dynamics (c and d panels).

Panel a clearly shows that an increase of the stretching frequency $\omega_s = \omega'_s$ increases the effectiveness of the dynamical trapping in such a way that at $\omega_s \geqslant 1.4 \times 711\ cm^{-1} \approx 1{,}000\ cm^{-1}$ almost no trajectory escapes the NR region. An analysis of the Lyapunov exponents obtained with $k = 1.6$ for the same initial conditions of Fig. 2, shows that the fraction of chaotic trajectories is much less than for $k = 1.0$. This finding supports the validity of the link we stressed above: the more regular is the dynamics the more effective is the trapping. Moreover, it is shown that $P_{NR}(t)$ is very sensitive to the potential in the range $0.9 < k < 1.2$, which includes the parameter $k = 1.0$, corresponding to the model of [20]. It is interesting to notice that the larger sensitivity of the dynamical trapping of classical trajectories with null initial momenta in the $0.9 < k < 1.2$ range is well reproduced by a crude but suggestive model based on a

Mathieu equation, obtained assuming that x_s follows an unperturbed harmonic motion.[1]

Comparison of panels b and a confirms what we stated in the previous section for the case $k = 1.0$, i.e. that the introduction of the distribution of the momenta always decreases the fraction of the trapped trajectories, and once more it shows that $P_{NR}(t)$ is more sensitive to k in the range $0.9 < k < 1.2$. Comparison of panels b and c shows that, for the same k, the classical (WD) and quantum results are practically coincident up to $t = 80$ fs. For longer times, there is a difference that increases when k increases. The classical $P_{NR}(t)$ decay stop in about 200 fs to a finite not-null value (a fraction of the trajectories is permanently trapped). Of course, when considering the possible effect of other nuclear modes, this trapped part might also decay toward the CI but to a much lower rate resulting into a multi-exponential decay. A correct quantum mechanical calculation eliminates the trapping effect showing that, after a first induction period of about 20 fs, the quantum $P_{NR}(t)$ always decays to zero, although the decay-rate decreases with increasing k. This puts into evidence a substantial difference between the quantum results and their classical approximation. The reason for this classical/quantum discrepancy is probably due to the well-known deficiency of the LSC-IVR semi-classical approach in the description of tunnelling phenomena [30], which in the present case are not due to a potential barrier but to a dynamical effect. Our results are somewhat reminiscent of those obtained by Heller and Davies [31] in the study of resonances in molecular spectra of non-harmonic bi-dimensional systems, and as a matter of fact our potential V^C in Eq. (1) can be seen as a particular case of the one they studied (it includes an additional term $1/2m_t\Omega_t^2 y_t^2$, that in our case is zero, $\Omega_t = 0$). In the cases studied in [31], the potential supports bound states and, while classical trajectories are confined in particular regions of the phase-space, local quantum states couple showing spitted doublets which the authors interpret as due to a dynamical barrier and the consequent quantum tunnelling. On the contrary, our potential V^C in Eq. (1) does not support any bound state and the dynamical barrier which traps a fraction of classical trajectories in the plateau region is unable to confine the quantum wavepacket motion.

[1] The equation of motion along the y_t co-ordinate becomes then a Mathieu equation, whose characteristic exponent is $x_s(0)(\omega_t/\omega_s)^2$. For $x_s(0) = -1$ au, and the assumed frequency ratio ($k = 1$) we are just at the borderline between bound and unbound motion along y_t (real and complex exponent, respectively). Surprisingly such sensitivity in this region of k values is still present, even if greatly reduced, also in the correct quantum dynamics.

Semi-log plots in panel d show that quantum $P_{NR}(t)$ decays approximately as a mono-exponential but evidence some marks of a bi-exponential decay, particularly for $k = 1.2, 1.4, 1.6$. As an example for the cases $k = 1.2, 1.6$, Table 1 reports the results of the bi-exponential fit showing that is about ten times better than a mono-exponential one.

3.6 Effect of a small barrier along the torsional coordinate

In ref. [8], we showed that for the specific parameters of PSBR ($\omega_s = 1{,}500$ cm^{-1} and $\omega_t = 200$ cm^{-1}), the introduction of a small barrier (about 200 cm^{-1}) on the PES along the *cis–trans* torsional deformation at $x_s > 0$, is able to offset the momentum effects which, as we have seen above, contrast the trapping phenomenon, and induce a multi-exponential decay of the quantum $P_{NR}(t)$. Here we inquire if such a phenomenon occurs also for very different potential parameters (namely $\omega_s = 711$ cm^{-1} and $\omega_t = 503$ cm^{-1}), being thus a general feature of the dynamics on a wide plateau. This scenario would be of general interest since even top-quality quantum chemical calculations can fail to distinguish a barrierless plateau from a plateau modulated by a barrier of very few hundreds of wavenumbers in medium-size molecules. Furthermore barriers of this kind could also come out as an effect of the environment in which the molecule is embedded.

In order to introduce a barrier in the original PES, we have modified the functional form of $V^C(x_s, y_t)$ in Eq. (1) to get $V^B(x_s, y_t)$, a new and more flexible PES. Accordingly, the $1/2m_t\omega_t^2 x_s y_t^2$ term in Eq. (1) has been substituted with

$$F(x_s, y_t) = \frac{f_2(y_t) + f_1(y_t)\exp[-\gamma x_s]}{1 + \exp[-\gamma x_s]}, \tag{4a}$$

$$f_1(y_t) = 1/2m_t\omega_t^2 y_t^2, \tag{4b}$$

$$f_2(y_t) = p_t\left(2\exp[-1/\alpha_y^2] - \exp[-(y_t - y_t^m)^2/\alpha_y^2 - (y_t + y_t^m)^2/\alpha_y^2]\right), \tag{4c}$$

$$V^B(x_s, y_t) = 1/2m_s\omega_s^2 x_s^2 - x_s F(x_s, y_t) \tag{4d}$$

$V^B(x_s, y_t)$ is negligibly different from V^C in the half-plane $x_s < 0$, retains a plateau around the origin and, in the $x_s > 0$ half-plane, at variance with V^C shows a barrier along y_t, whose height (with respect to $y_t = 0$) is zero at $x_s = 0$ and then increases almost linearly with x_s depending on the parameter α_y. The barrier location is practically constant with x_s. With respect to x_s, $F(x_s, y_t)$ is a switching function which gives $f_1(y_t)$[the same as in Eq. 1] when $x_s < 0$ and turns it smoothly into $f_2(y_t)$ when $x_s > 0$; the value of γ is chosen so to ensures a switch

fast enough to make the new potential V^B only negligibly different from V^C in the half-plane $x_s < 0$. Despite its lengthiness, $f_2(y_t)$ is just a combination of two gaussian functions, written in a way to ensure that $f_2(0) = 0$. The frequencies and masses are those utilized in [20] and in Sect. 3.1 to 3.4, while the values of the new parameters introduced in Eqs. (4a), (4b), (4c) and (4d) are $y_t^m = 1$ au, $p_T = 0.1$ au and $\gamma = 5$ au and we have tested two different choices $\alpha_y = 1.8$ au and $\alpha_y = 1.7$ au, that give, respectively, a maximum accessible barrier height ($B^{\max}$), at the turning point $x_s = 1.0$ au, of 205 cm^{-1} (located at $y_t = 0.53$ au) and of 475 cm^{-1} (located at $y_t = 0.63$ au). In Fig. 1b, $V^B(x_s, y_t)$ is plotted for the case $B^{\max} = 205$ cm^{-1}, and it is compared with the original potential $V^B(x_s, y_t)$ of Fig. 1a (see also SM for other plots). For $x_s > 0$, at y_t values larger than the position of the barrier, V^B decreases steeper than V^C but this is of no consequence for our study.[2]

Figure 6 shows the plot of the $P_{NR}(t)$ evolution on V^C and on the modified potential V^B with the two choices $B^{\max} = 205$ cm^{-1} and $B^{\max} = 475$ cm^{-1} and the inset reports the semi-log plot. It is seen that the three curves are almost coincident up to 40 fs and then they start diverging since, while the curve for V^C in the semi-log plot keeps an approximately constant slope (mono-exponential decay) the two curves for V^B change clearly to a different slope (bi-exponential decay) whose magnitude, quite intuitively, decreases with the increase of the barrier. These conclusions are supported by comparison of the best mono- and bi-exponential fits reported in Table 1, which shows that the existence of a very small barrier greatly amplifies the weak signs of multi-exponential behaviour already seen in the case on the V^C potential and leads to a clear bi-exponential decay. For the case of potential V^B with $B^{\max} = 205$ cm^{-1}, 1/4 of $P_{NR}(t)$ decays very quickly with $\tau_1 = 16$ fs and the rest decays more slowly with a $\tau_2 = 184$ fs. Increasing the barrier to $B^{\max} = 475$ cm^{-1}, the faster decay rate is almost unaltered ($\tau_1 = 17$ fs) but now it concerns about 1/5 of $P_{NR}(t)$ while the remaining part decays with $\tau_2 = 363$ fs, which is slower, as intuitive, than in the case when the barrier is smaller. The faster decay of $P_{NR}(t)$ is accomplished during one oscillation period along the stretching coordinate (46.9 fs), and hence it is due to the wings of the $|FC\rangle$ wave packet that at the first passage at $x_s > 0$ elongate toward the decay channels (this also explains why the amount of population decaying at faster rate is smaller for the case $B^{\max} = 475$ cm^{-1}, since in this case the barrier is shifted more along y_t and a littler amount of $|FC\rangle$ can initially escape it). At each of the subsequent oscillations, a smaller percent of the surviving part of the wave packet enters the decay channels giving rise to the second slower decay.

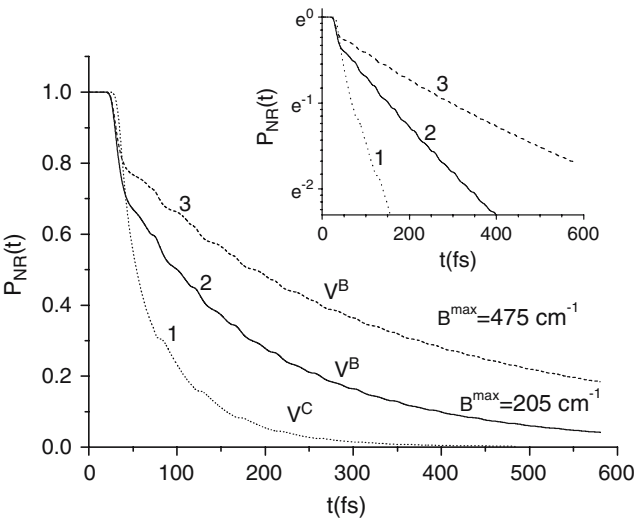

Fig. 6 Plot of the decay of the quantum non-reactive wave packet population on V^C *(1)*, on V^B with $B^{\max} = 205$ cm^{-1} *(2)* and on V^B with $B^{\max} = 475$ cm^{-1} *(3)*. In the inset semi-log plot. Best fit data are reported in Table 1 and figures comparing the data and their fits are reported in the Supporting Material

In Fig. 7, we show some snapshots of the probability density of the wave packet moving on the potential with the lower barrier $B^{\max} = 205$ cm^{-1}, taken at the same times as in Fig. 4, with whom Fig. 7 should be compared. The corresponding wave packets are identical at $t = 0$ and are still very similar at $t = T_s/4$. On the contrary, at $t = 3T_s/4$ the part of the wave packet crossing the borders on V^C seem to be larger than the corresponding quantity for the wave packet moving on V^B. Consistently, the data in Fig. 6 indicates that it is about at these times that the decay of $P_{NR}(t)$ for V^C starts being faster than that for V^B. The situation does not change in the next snapshot when one period of the oscillation along x_s is over. Because of the barrier it felt at $x_s > 0$, the wave packet that starts the second oscillation on V^B is much less elongated than the one that moves on V^C and this explains why at later times a smaller part of it crosses the borders (look especially the snapshots at $t = 5T_s/4$ and $t = 6T_s/4$). Moreover, the differences in the dynamics on the V^C and V^B potentials are permanent since each oscillation is similar to the previous one and the $t = 2T_s$ and $t = 3T_s$ wave packet closely

[2] In fact, though this feature causes some slight anticipation on the times at which the border of the NR non reactive region is crossed and gives some different preferential orientation to the part of the wave packet travelling toward the borders (due to orientation of the forces it feels), this is of no relevance for our interest here, since the change occurs in a region where in any case the wave packet is irreversibly accelerate to escape from the NR region.

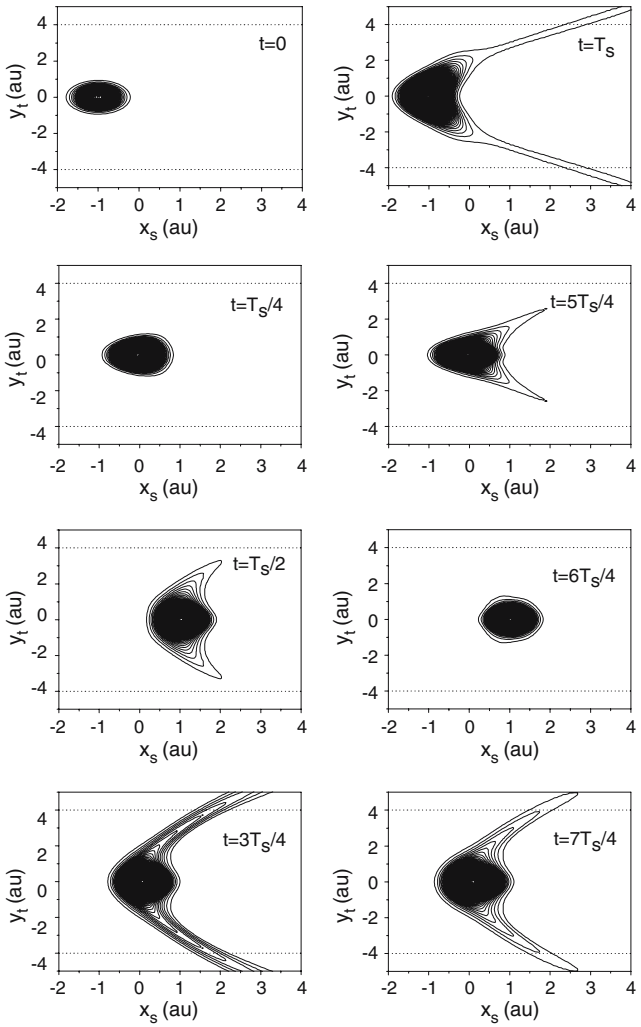

Fig. 7 Snapshots of the quantum wave packet running on $V^B(B^{\max} = 205\ \mathrm{cm}^{-1})$ at different times, reported as fractions of the stretching period T_s. Notice that, for a better comparison, before plotting, the part of the wave packet not yet absorbed at the borders of the grid has been re-normalized (see Supporting Material for the normalization factors)

resemble the shape it had at $t = T_s$. These differences indicate that the dynamics of the wave packet on V^B has entered a different time regime, giving rise to the slower decay of $P_{NR}(t)$ described by the slower component of the bi-exponential fit reported in Table 1.

4 Conclusions

In this paper, we have extensively investigated the dynamical consequences of a plateau on the excited PES, like the one predicted by highly accurate CASSCF method for PSBR [1–3]. We utilized a simple 2D analytical expression V^C for the PES and varied its parameters.

The study of the classical motion of individual trajectories on V^C with the same parameters used in [20] has shown evidence for dynamical chaos, enlightening a clear correlation between the regularity of a single trajectory and the time duration of its trapping in the plateau region (the smaller is its Lyapunov exponent the longer is the trapping). On the other hand, quantum dynamics has shown that, on the barrierless V^C potential, the trapping is not effective anymore at quantum level. Indeed, the wave packet decays entirely and about mono-exponentially in the reactive channels and the classical simulations suggest that this is due to the role of the initial momentum distribution, which destroys the regular trajectories that would remain trapped if starting with zero-momentum (as in [20]).

Nevertheless, this explanation is only partial since, by varying the parameters of the PES, we report several cases where a significant fraction of classical trajectories is trapped even when their initial conditions correctly simulate a wave packet (i.e. when also the initial momenta distribution is properly taken into account). This shows a net discrepancy with quantum results which, for all the barrierless PESs considered, always predict a complete depletion of the non-reactive population according to a law approximately mono-exponential (or weakly bi-exponential), although the decay-rate changes with the potential parameters.

The comparison of quantum and classical results show that the dynamics on V^C is very rich and complex, suggesting that, although not sufficient at quantum level, the existence of the plateau is the essential ingredient for the occurrence of a multi-exponential decay. The classical trajectories study is very instructive in so for it indicates that the trapping is made more difficult by the initial momenta distribution of the wave packet. This naturally suggests that a small barrier contrasting these momenta might restore the condition for trapping, creating consequently a situation more favourable to the appearance of a bi-exponential decay. We have shown that this is indeed true and, in fact, when the shape of the PES plateau is changed, introducing a shallow barrier toward the decay channels, a bi-exponential decay is observed also at quantum level. For a torsional frequency of $\sim$500 cm^{-1}, a very small barrier of $\sim$ 200 cm^{-1} is enough to induce the change in the decay- law.

The clear discrepancy between quantum results and their classical approximation (WD) obtained for some choices of the potential parameters has an interest in itself, and suggests that, for potential surfaces exhibiting large plateaux, any attempt to avoid quantum propagation can lead to significant errors.

In future work we plan to investigate the role of the environment on the dynamics on such a model system. In particular, since the wave packet noticeably spreads on the PES, it will be interesting to address the role of de-coherence effects.

Acknowledgments MO acknowledges the Università di Siena (Progetto di Ateneo 02/04), HFSP (RG 0229/2000-M) and FIRB project No. RBAU01EPMR for providing the funds.

Electronic supplementary material

A figure comparing the potential $V^C(\omega_s = 711\,\mathrm{cm}^{-1}$ and $\omega_t = 503\,\mathrm{cm}^{-1})$ with $V^B(B^{\max} = 205$ and $475\,\mathrm{cm}^{-1})$. Figures comparing the performance of mono-exponential and bi-exponential fits for the first 3 cases reported in Table 1; a table with the normalization factors adopted in Figs. 4 and 7.

References

1. Garavelli M, Celani P, Bernardi F, Robb MA, Olivucci M (1997) J Am Chem Soc 119:6891
2. Garavelli M, Vreven T, Celani P, Bernardi F, Robb MAM, Olivucci M (1998) J Am Chem Soc 120:1285
3. Gonzalez-Luque R, Garavelli M, Bernardi F, Merchan M, Robb MA, Olivucci M (2000) Proc Natl Acad Sci USA 97:9379
4. Improta R, Santoro F (2005) J Chem Theor Comp 1:215
5. Migani A, Robb MA, Olivucci M (2003) J Am Chem Soc 125:2804
6. Hunt PA, Robb MA (2005) J Am Chem Soc 127:5720
7. Nangia S, Truhlar DJ (2006) J Chem Phys 124:124309
8. Olivucci M, Lami A, Santoro F (2005) Angew Chem Int Ed 44:5118
9. Hamm P, Zurek M, Röschinger T, Patzelt H, Oesterhelt D, Zinth W (1996) Chem Phys Lett 263:613
10. Logunov SL, Song L, El-Sayed M (1996) J Phys Chem 100:18586
11. Yan M, Rothberg L, Callender R (2001) J Phys Chem B 105:856
12. Kandori H, Furutani Y, Nishimura S, Shichida Y, Chosrowjan H, Shibata Y, Mataga N (2001) Chem Phys Lett 334:271
13. Schenkl S, Portuondo E, Zgrablic G, Chergui M, Haacke S, Friedman N, Sheves M (2002) Phys Chem Chem Phys 4:5020
14. Zhong Q, Ruhman S, Ottolenghi M (1996) J Am Chem Soc 118:12828
15. Hou B, Friedman N, Ruhman S, Sheves M, Ottolenghi M (2001) J Phys Chem B 105:7042
16. Song L, El-Sayed MA (1998) J Am Chem Soc 120:8889
17. Haran G, Morlino EA, Matthes J, Callander RH, Hochstrasser RM (1999) J Phys Chem A 103:2202
18. Haacke S, Vinzani S, Schenkl S, Chergui M (2001) Chem Phys Chem 2:310
19. Kobayashi T, Saito T, Ohtani H (2001) Nature 414:531
20. Cembran A, Bernardi F, Olivucci M, Garavelli M (2003) J Am Chem Soc 125:12509
21. Kukura P, McCamant DW, Yoon S, Wandschneider DB, Mathies RA (2005) Science 310:1006
22. Kosloff R (1996) In: A Dynamics of molecules and chemical reactions. Wyatt RE, Zhang JZH (eds) Marcel Dekker, Inc., New York.
23. Lanczos C (1950) Res Nat Bur Stand 45:225
24. Ferretti A, Granucci G, Lami A, Persico M, Villani G (1996) J Chem Phys 104:5517
25. Gray SK, Balint-Kuri GG (1997) J Chem Phys 108:950
26. Benettin G, Galgani L, Strelcyn J-M (1976) Phys Rev A 14:2238
27. Balzer B, Dithley S, Stock G, Thoss M (2003) J Chem Phys 119:5795
28. Balzer B, Dithley S, Hahn S, Thoss M, Stock G (2003) J Chem Phys 119:4204
29. Sun X, Wang H, Miller WH (1998) J Chem Phys 109:7064
30. Wang H, Sun X, Miller WH (1998) J Chem Phy 108:9726
31. Davies MJ, Heller EJ (1981) J Chem Phys 75:246